JOURNAL OF GEOPHYSICAL RESEARCH, VOL. 103, NO. D18, PAGES 23,087–23,101, SEPTEMBER 27, 1998

Snow breezes in the boreal forest

Christopher M. Taylor, Richard J. Harding
Institute of Hydrology, Wallingford, England

Roger A. Pielke Sr., Pier L. Vidale, and Robert L. Walko
Colorado State University, Fort Collins

John W. Pomeroy
National Hydrology Research Institute, Saskatoon, Saskatchewan, Canada

Abstract. This study examines thermally induced flows (or "snow breezes") associated with snow cover in the boreal forests of Canada. Observations from a lake less than 4 km across were made as part of the Boreal Ecosystem-Atmosphere Study (BOREAS) winter field campaign. These are interpreted with the aid of idealized three-dimensional mesoscale model simulations representing the forest-lake contrast. Typically, strong forest-lake temperature contrasts develop in the lowest 50 m of the atmosphere during the morning. The resulting pressure gradients induce low-level onshore wind components across the lake. This snow breeze persists into the afternoon provided that large-scale winds remain light. A characteristic snow breeze signature is clearly evident in wind observations averaged over 27 days of data, in agreement with model simulations. The study suggests that snow breezes will regularly develop over the many larger lakes and other unvegetated areas in the region.

1. Introduction

Variations in the land surface can have a marked influence on the properties of the planetary boundary layer (PBL). The effect of contrasting surface fluxes of heat, moisture, and momentum depends on spatial scale [*Shuttleworth*, 1988]. At scales of less than a few kilometers (or microscale) [*Raupach and Finnigan*, 1995], the effect of variability in fluxes on the atmosphere may be blended out near the surface [*Mason*, 1988]. On the other hand, the entire depth of the PBL can be affected by mesoscale heterogeneity. In this case if the surface variability is associated with strong horizontal gradients in sensible heat flux, thermally forced "non classical mesoscale circulations" (NCMCs) can develop [*Segal and Arritt*, 1992].

Nonclassical mesoscale circulations have been the focus of a number of idealized studies [e.g., *Ookouchi et al.*, 1984; *Pinty et al.*, 1989; *Mahfouf et al.*, 1987; *Pielke et al.*, 1991; *Segal et al.*, 1988; *Dalu et al.*, 1991; *Segal et al.*, 1991b]. These have illustrated how mesoscale patterns of soil moisture, snow, and vegetation cover can generate and modulate PBL flow. The development of NCMCs is very sensitive to the contrast in surface heat fluxes between adjacent patches, the length scale of the patches, and the large-scale wind. In particular, mesoscale circulations are favored by light ambient wind conditions and strongly contrasting patches several tens of kilometers across [e.g., *Segal and Arritt*, 1992]. A number of authors have argued that vertical fluxes associated with NCMCs are an important transport mechanism requiring parameterization in general circulation models [*Pielke et al.*, 1991; *Lynn et al.*, 1995; *Zeng and Pielke*, 1995]. Other papers have examined the role of NCMCs on the initiation and development of storms [*Sun and Ogura*, 1979; *Chang and Wetzel*, 1991, *Chen and Avissar*, 1994]. As noted by *Segal and Arritt* [1992], observational studies of NCMCs are scarce [*Segal et al.*, 1989; *Segal et al.*, 1991a; *Mahrt et al.*, 1994; *Smith et al.*, 1994]. This is partly due to the shortage of appropriate mesoscale observations but also through the masking of a circulation signal by topographic and large-scale flows. *Zhong and Doran* [1997] argue however that the lack of clear observational evidence indicates that under real world conditions, NCMCs are not so widespread as predicted by idealized modeling studies.

The Boreal Ecosystem-Atmosphere Study (BOREAS) [*Sellers et al.*, 1995] provides the opportunity to examine the occurrence of NCMCs in the boreal forests of Canada. Summer airborne observations [*Sun et al.*, 1997] have shown how lakes within the forest provide surface heating contrasts sufficient to induce lake breezes. Detailed modeling studies using realistic surface parameters [*Vidale et al.*, 1997] have supported these result findings. The study of heterogeneity in the BOREAS region is extended in this work to the winter and spring months. At this time, the region is snow covered, with lakes frozen over, insolation low, and temperatures as low as -40°C. In this case, heterogeneity is provided by the contrasting characteristics of the forest with open snow cover lying on lakes and in other unvegetated areas such as open wetlands and over agricultural and recreational development. These areas may be considered to cover about 30% of the region. This raises the possibility of NCMCs induced by the presence of open snow cover within the forest, or "snow

Paper number 98JD02004.
0148-0227/98/98JD-02004$09.00

breezes". "Frozen lake breezes" may also occur in the region when snow has melted off the lake surfaces. As frozen lake breezes are similar to snow breezes [*Segal and Kubesh* 1996], only the latter will be treated here.

Observational evidence for snow breezes is presented here from measurements taken during a field campaign in March and April 1996 as part of BOREAS. For logistical reasons the observations were made across one of the numerous relatively small lakes, approximately 4 km across. At this length scale, snow breezes are expected to be weak and may be masked by other atmospheric features. A mesoscale model was therefore used to interpret the observations.

The observational study area is described in section 2, along with an outline of the measurements taken. Characteristic differences in the surface energy balances of forests and frozen lakes are shown. Section 3 provides a summary of the numerical model, with an emphasis on the parameterization of surface fluxes from snow-covered surfaces. A case study of a snow breeze case under light wind conditions is presented in section 4. The observations are interpreted with the aid of a model simulation. Observations and idealized simulations are analyzed in section 5 under a range of wind conditions. This gives an indication of how frequently snow breezes occur in the region.

2. Description of Surface and Observations

2.1. Observational Network Around Namekus Lake

The observation campaign took place on Namekus Lake, Saskatchewan (53°52'N, 106°8'W) in Canada between March 7 and April 11, 1996. The study area is within Prince Albert National Park, depicted in Figure 1. Namekus Lake is roughly circular, with a 3.5 km diameter, and is set among a mixed-wood forest containing jack pine, black spruce, and aspen. Within the National Park, very little forest has been cleared, though clear-cuts are extensive elsewhere in the region. There are a number of smaller neighboring lakes, and the larger Waskesiu Lake 10 km to the northwest. The surrounding terrain is fairly flat, although a small hill rises 100 m above the lake 3 km to the northwest. Observations are also available from a jack pine forest site near Beartrap Creek, some 7 km northwest of Namekus Lake.

Spatial variability in the surface layer was sampled at three sites across Namekus Lake (Figure 1b). Three anemometers and wind vanes were installed at a height of 2 m above the snow surface approximately 500 m from the northwestern, southwestern, and eastern shores. In addition, temperature, radiation and turbulent surface fluxes were recorded at the northwestern site. Further measurements of radiation, wind, turbulent fluxes, and temperature were made at the nearby Beartrap forest site. Over a period of 10 days (March 12 - 21), a tethered balloon system (AIR Inc., Boulder, Colorado) was installed on the lake at a location 750 m from the northwestern shore. This system provided temperature and wind speed and direction measurements every 10 s to heights of several hundred meters. To ensure a stable platform for the measurements, ascents for were only made when winds were generally less than 6 ms^{-1}. Observations were possible on 7 out of the 10 days.

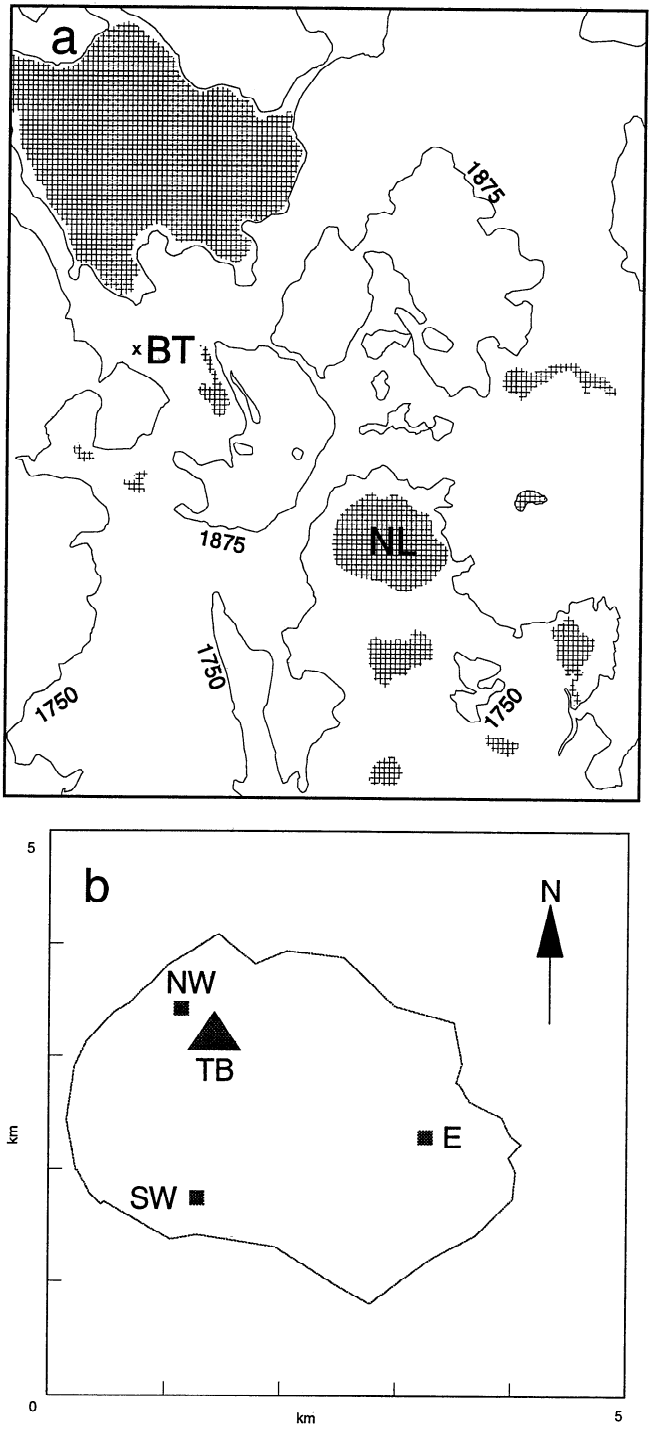

Figure 1. (a) Study area in Prince Albert National Park showing lakes (hatched) and height contours every 125 feet (38 m). The observational sites at Beartrap (BT) creek and Namekus Lake (NL) are marked. (b) Observational network over Namekus Lake showing the tethered balloon site (TB) and the locations of the three anemometers near the northwestern, southwestern, and eastern shores.

2.2. Winter Surface Energy Balances

The Beartrap forest site is in a stand of mature jack pine (*Pinus banksia*) with a height of typically 20 m, leaf area index of 2.2 m^2/m^2, and canopy coverage of 82%. The surface energy balance has been characterized by *Harding and Pomeroy* [1996] and *Pomeroy and Dion* [1996] from measurements made in 1994. Despite the presence of snow on the frozen forest floor throughout the winter months, the net albedo of the forest is low (0.10-0.16), depending on solar angle. Following snowfall, substantial latent heat fluxes

can arise from sublimation of intercepted snow on the canopy. During the cold, low-radiation midwinter, intercepted snow can remain on the lower canopy for several weeks. However, in general, turbulent fluxes above the canopy are dominated by sensible heat. For example, during the daytime period in the months of March and April 1996, 40% of the incoming solar radiation above the canopy was converted to sensible heat fluxes, including days when intercepted snow was present. The large sensible heat fluxes are due to a high roughness length, frozen soils preventing transpiration and evaporation, and poor coupling between the forest floor and the PBL.

The lake energy balance contrasts strongly with that of the forest [*Harding and Pomeroy*, 1996]. Observations on Namekus Lake show that albedos during the winter range between 0.7 and 0.9, while roughness lengths typically take values ~1 mm, depending on the wetness of the snow and ice exposure. Blowing snow occurs on open surfaces when wind speeds exceed a threshold value. Average threshold speeds of 7.7 ms^{-1} at 10 m have been reported by *Li and Pomeroy* [1997] for dry snow, increasing when the snow is wet. During blowing snow events, turbulent transfers with the surface are greatly enhanced, resulting in episodic negative sensible heat fluxes as large as 100 W m^{-2}. Averaged over the entire 1996 campaign however, downward daytime sensible heat fluxes are small, only 1.4% of the incoming short wave energy.

3. Numerical Model

In this study, the Regional Atmospheric Modeling System (RAMS) [*Pielke et al.*, 1992] is adopted to examine the atmospheric interactions between the forest and the frozen lake. This three-dimensional mesoscale model has been used widely to investigate surface-induced circulations [e.g., *Pielke et al.*, 1991]. The model was run with a horizontal grid length of 375 m over a domain of 38 x 46 grid points. A series of fully interactive nested grids at coarser resolution extend the domain over 100 km in the horizontal. The vertical grid spacing increases from 5 m above the surface by a factor of 1.1 with each level up to a height of 4 km. Water vapor is carried by the model, but no condensation processes are permitted. Subgrid turbulent mixing is based on a first-order deformation parameterization [*Smagorinsky*, 1963]. The mixing length and stability corrections employed in the vertical diffusion coefficients are taken from *McNider and Pielke* [1981]. A more detailed description of the land surface scheme is outlined below.

3.1. Surface Scheme

The land ecosystem-atmosphere feedback (LEAF-2) model [*Walko et al.*, 1998]) was used. This includes a multilayer snow and soil model, with a two source surface flux scheme. Of particular relevance here is the parameterization of surface fluxes from boreal land cover types during the winter.

The temperatures of a vegetation layer T_v and a snow-covered ground layer T_s are treated separately and coupled to a canopy space air temperature and mixing ratio T_c and χ_c. The vegetation temperature in the model is found from a balance of net short and long wave radiation (S_v and L_v respectively) and sensible heat flux from the vegetation to the canopy (H_{vc}) with an areal heat capacity of the forest C_v providing a thermal inertia term.

$$-C_v\frac{\partial T_v}{\partial t} = H_{vc} - L_v - S_v \tag{1}$$

It is important to note that this expression assumes that intercepted snow has a negligible effect on the energy balance. This condition restricts the use of the scheme to days when there is no snow on the upper canopy, in particular in the days following snowfall.

The top snow level energy balance is expressed in terms of water content per unit area of snow (and liquid water if melting) W and a variable Q representing the total thermal energy associated with the snow (and possibly water) at temperature T_s, including a latent heat term to account for changes of phase. In addition to the net long and short wave radiation terms L_s and S_s, the balance includes sensible and latent heat fluxes H_{sc} and λE_{sc} to the canopy space and a heat flux term to the next highest snow level G.

$$-\frac{\partial QW}{\partial t} = H_{sc} + \lambda E_{sc} - L_s - S_s - G \tag{2}$$

The fluxes to the canopy air space from the snow and the vegetation are given by

$$E_{sc} = \frac{\rho c_p (\chi_s - \chi_c)}{r_d} \tag{3}$$

$$H_{sc} = \frac{\rho c_p (T_s - T_c)}{r_d} \tag{4}$$

$$H_{vc} = \frac{\rho c_p (T_v - T_c)}{r_b} \tag{5}$$

where ρ and c_p are the density and heat capacity of the air, and the resistances r_b and r_d depend on characteristics of the surface.

Radiation transfer within the forest canopy is a complex subject [*Pomeroy and Dion*, 1996]. Developed for a range of vegetation types, the scheme in LEAF-2 treats the radiation rather simplistically, ignoring factors such as the strong dependence of albedo on Sun angle. The net short wave radiation fluxes absorbed by the vegetation S_v and snow S_s are given by

$$S_v = S_d \,\mathrm{veg}\,(1 - \alpha_v + \alpha_s(1 - \mathrm{veg})) \tag{6}$$

$$S_s = S_d\,(1 - \mathrm{veg})\,(1 - \alpha_s) \tag{7}$$

where S_d is downward solar radiation, α_v and α_s are the albedos of the vegetation and snow, respectively, and the vegetation covers a fraction *veg* of the surface area. Ignoring multiple reflections and assuming that snow has an emissivity of unity, the net long wave components for the vegetation L_v and snow L_s are

$$L_v = L_d\varepsilon_v \mathrm{veg} + \sigma\varepsilon_v \mathrm{veg}(T_s^4 - 2T_v^4) \tag{8}$$

$$L_s = L_d(1 - \mathrm{veg}) - \sigma T_s^4(1 - \mathrm{veg}) + \sigma\varepsilon_v \mathrm{veg}(T_v^4 - T_s^4) \tag{9}$$

The canopy air temperature and mixing ratio are coupled to the first atmospheric level using similarity theory, with transfers characterized by a net roughness length for the surface, z_0. For the case of a homogeneous surface such as the snow-covered lake, the two source scheme above collapses to a single snow energy balance with *veg*=0. The stability corrections of *Louis et al.* [1981] are adopted, and

Table 1. Surface Model Parameters describing Jack Pine Forest and Snow-Covered Lake.

	α_v	α_s	*veg*	z_0 (m)	r_d	r_b
Forest	0.12	0.64	0.82	1.0	120./u_*	35.
Lake	-	0.72	0.0	0.001	-	-

these agree closely with the formulation of *Male and Granger* [1978] which has been widely used for snow cover. The various parameter values and resistance formulations for the forest and lake surfaces are given in Table 1 and have been derived from observations [*Harding and Pomeroy,* 1996].

The simplifying assumptions made in this implementation of LEAF-2 for the boreal forest mean that the seasonal course of snow accumulation will be poorly simulated. However, comparison with observations suggest that the diurnal course of turbulent fluxes above the canopy are well represented. In addition, the use of a constant roughness length over the lake is inappropriate for conditions of blowing snow.

3.2. Model Initialization

The objective of the numerical modeling is to explore the diurnal evolution of the PBL around an idealized circular frozen lake of diameter 3.75 km, surrounded by a uniformly flat forest. These dimensions are intended to represent Namekus Lake. The idealized conditions were adopted as more realistic surface parameter maps at the spatial resolution required were not available.

The atmosphere was initialized homogeneously in the horizontal from a single vertical profile of temperature, humidity, and wind. The model was run from 0600 to 2000 LT (1200 to 0200 UTC), covering the daytime period when lake and forest heat fluxes are strongly contrasting. The snow was modeled with three layers assumed to have a constant density of 250 kg m^{-3} and a total depth of 300 mm. On the timescales considered here, the atmosphere is insensitive to the details of snow initialization.

4. Case Study, March 12, 1996

In this section, an observational case study of a snow breeze at Namekus Lake is presented. Of the 10 days when the tethered balloon system was operating, March 12 was chosen because it presented the most favorable atmospheric conditions for snow breezes. To complement the observations, the numerical model is used to examine the forest-lake interactions under these meteorological conditions.

4.1. Observations

With temperatures at the nearby Beartrap forest site reaching 12°C, March 12 was the third day in succession when snowmelt occurred. The sky was initially clear, with scattered shallow cumulus appearing in late morning. Northwesterly winds ~ 3 ms^{-1} strengthened to a speed of 7 ms^{-1} by 1400, preventing subsequent balloon ascents. The balloon measurements provide an indication of the vertical structure of the PBL roughly 750 m downwind of the forest-lake transition. Hourly ascents up to 200 m were made between 1000 and 1400, with a number of shallower profiles recorded in the intervening times.

The evolution of the stable layer above the lake is illustrated by the hourly profiles in Figure 2. At 1000 the temperature profile indicates strongly stable conditions up to a height of 60 m, with the largest thermal gradients occurring in the lowest 10 m. In the following hour, warm air advected off the forest gradually eroded the stable layer from above. Subsequently, the potential temperature profiles were fairly well mixed above 10 m. However, beneath the lowest balloon measurement (2 m), the profile remained extremely stable throughout the day, with the frozen lake surface temperature unable to rise above 0°C (equivalent to a potential temperature of 4.4°C). This intense temperature gradient was visible as a "heat haze" just above the lake surface during the afternoon.

The balloon observations of offshore wind profiles are less easy to interpret than the temperature data. This is due primarily to the transience of the wind field. Time-averaging techniques were attempted to produce a smoother composite profile. However, the averaging period required for this often exceeded the time in which the temperature profile could be regarded as approximately constant. Instead, the once-hourly "snapshots" are shown in Figure 2. The representativeness of these wind conditions is provided qualitatively by reference to the balloon ascents made between the hours.

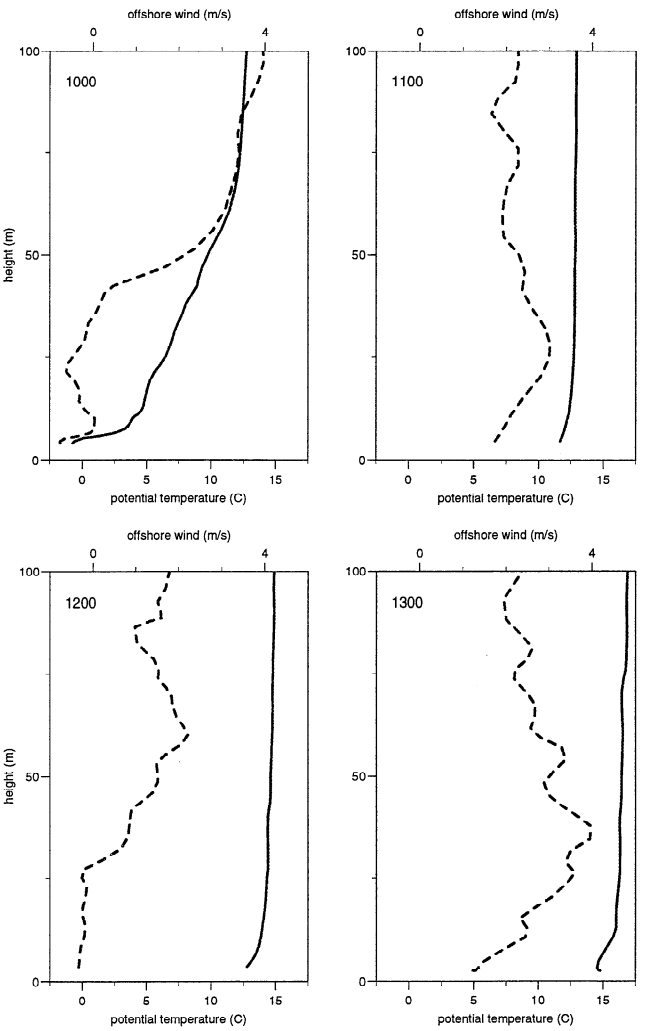

Figure 2. Hourly profiles of potential temperature (°C; solid) and offshore wind (ms^{-1}; dashed) on March 12. A three point filter has been applied to the wind data.

The 1000 profile is typical of the early morning conditions and shows a well-defined region of weak onshore flow beneath 50 m. This corresponds to the strongly stable layer and contrasts sharply with repeatedly observed offshore flow ~ 4 ms^{-1} aloft. The low-level onshore component gave way to offshore winds during the day as the temperature profile became more well mixed. However, it should be noted that during a period of lighter winds between 1145 and 1245 (~ 2 ms^{-1} at 60 m), other profiles indicated a strengthening of the inversion between 2 m and 20 m. This was accompanied by weak onshore wind components beneath 20 m, as is evident from the 1200 profile in Figure 2.

The spatial variability in low-level wind across the lake can be seen in Figure 3. This figure shows the hourly averaged wind vectors from the SW and E sites for the period when balloon profiles were available (note that the wind vane at the northwestern site was not functioning on this day). For comparison, the time-average winds observed by the tethered balloon between 45 m and 200 m are also shown. Prior to 1300, a marked low-level onshore component to the wind is evident at the SW and E sites. This is in contrast to the northwesterlies observed above the stable layer by the tethered balloon.

The observations suggest that the flow above the lake is influenced by a snow breeze. A strong inversion forms when warm forest air is advected over the lake. This prevents cool air at the lake surface from mixing upward and induces a near-surface pressure gradient. The wind at low levels is partly decoupled from the northwesterlies aloft, and onshore flow develops in response to the high pressure over the lake. However, when the wind speed aloft increases, the stable layer is eroded and the snow breeze dissipates. This qualitative description of March 12 is now examined quantitatively using the numerical model.

4.2. Model Simulation

The model is initialized from the 0600 (1200 UTC) atmospheric sounding at the Pas, Manitoba. Located 300 km to the east of Namekus Lake, this was the closest available observation. Above 500 m the profile is moderately stable, with wind speeds increasing from 5 ms^{-1} to 7.5 ms^{-1} at 3 km. For the purposes of model initialization the strongly stable profile at the Pas below 500 m is warmed throughout by several degrees. This is done to match local observations of temperature above the forest canopy and tethered balloon measurements of the residual layer above 100 m at 1000. The profile (Figure 2) indicates temperatures of 10°C at 150 m, implying an intense low-level inversion. The snow is initialized with a surface temperature of -7.5°C, increasing to -4.5°C at the bottom of the 300 mm pack in agreement with available observations.

The observed net radiation and sensible heat fluxes from the Beartrap forest site are shown in Figure 4. The turbulent sensible heat flux represents a little less than 50% of the net radiation absorbed by the forest canopy and underlying snow. With observed hourly latent heat fluxes never exceeding 40 W m^{-2} (not shown), the remaining energy is used to warm the forest canopy and snowpack, with melt rates in the afternoon corresponding to over 100 W m^{-2}. The numerical model produces significant differences in downward radiation at the surface compared to the observations. This is due to both the absence of clouds in the idealized simulation, and an underprediction of the clear-sky downward short wave component at the surface of up to 100 W m^{-2}. Despite these differences in forcing, the LEAF-2 scheme produces a similar partition of fluxes (Figure 4) to the measurements. As observed, the rise in model sensible heat flux lags the net radiation by an hour or so when the Sun comes up, due to the thermal inertia of the surface. During periods of clear skies the modeled sensible heat flux is similar to the observations.

Flux observations over the lake are not available for March 12, but values from the simulated lake 750 m downwind of the shore are shown in Figure 4. The sensible heat flux is very close to zero during the initially calm period and becomes slightly more negative as the near surface wind speed and temperature rise. The magnitude of the modeled lake heat flux is slightly sensitive to the initial conditions of the snowpack. However, it is clear from Figure 4 that even on such a warm day, when temperature gradients above the snow are large, the contrast in surface heating between forest and lake is determined by the absorption of radiation at the forest canopy.

The modeled evolution of the PBL over the contrasting surfaces can be seen in Figure 5. At 1000 (Figure 5a), sensible heating erodes the initially stable layer to a depth of 50 m above the forest. Above the lake surface however, a strong inversion persists in the absence of local surface heating. As a result, marked horizontal temperature gradients develop across the shoreline (Figure 5b). The thermal contrasts are constrained to the lowest ten meters in the vertical by the initial stable layer. The horizontal temperature gradients perturb the mixed layer westerly momentum, with the lowest 15 m characterized by onshore flow. The symmetry of the snow breeze is distorted in the direction of the large-scale wind. This is due to advection strengthening (weakening) the thermal gradients at the upwind (downwind) edge of the lake.

By 1300, turbulent mixing has eroded the inversion from above, with stable conditions restricted to the downwind side of the lake (Figure 5c). Across the upwind shore the low-level flow accelerates in response to the decrease in surface roughness. No snow breeze effect is apparent here, while on the colder eastern side, the wind direction remains primarily onshore. Following a further 3 hours in the simulation, the thermally induced pressure gradients have been advected downwind of the lake. Although the low-level wind still decelerates across the eastern half of the lake in response to the thermal forcing, the direction remains close to westerly everywhere.

4.3. Comparison of Observations With Model

In this section the available observations are compared with the numerical model to verify that the simulation captures the basic features of the PBL on March 12. A comparison of vertical temperature and momentum profiles at 1000 and 1300 is shown in Figure 6. The model diagnostics are taken from the grid point denoted by a circle in Figure 5, 750 m downwind of the shoreline. The transition in stability between 1000 and 1300 is clear in both model and observations (Figure 6a). However, the stable layer observed in the lowest 25 m at 1300 is not reproduced in the model. This inversion developed during the relatively calm period between 1145 and 1245 and was not apparent in subsequent ascents.

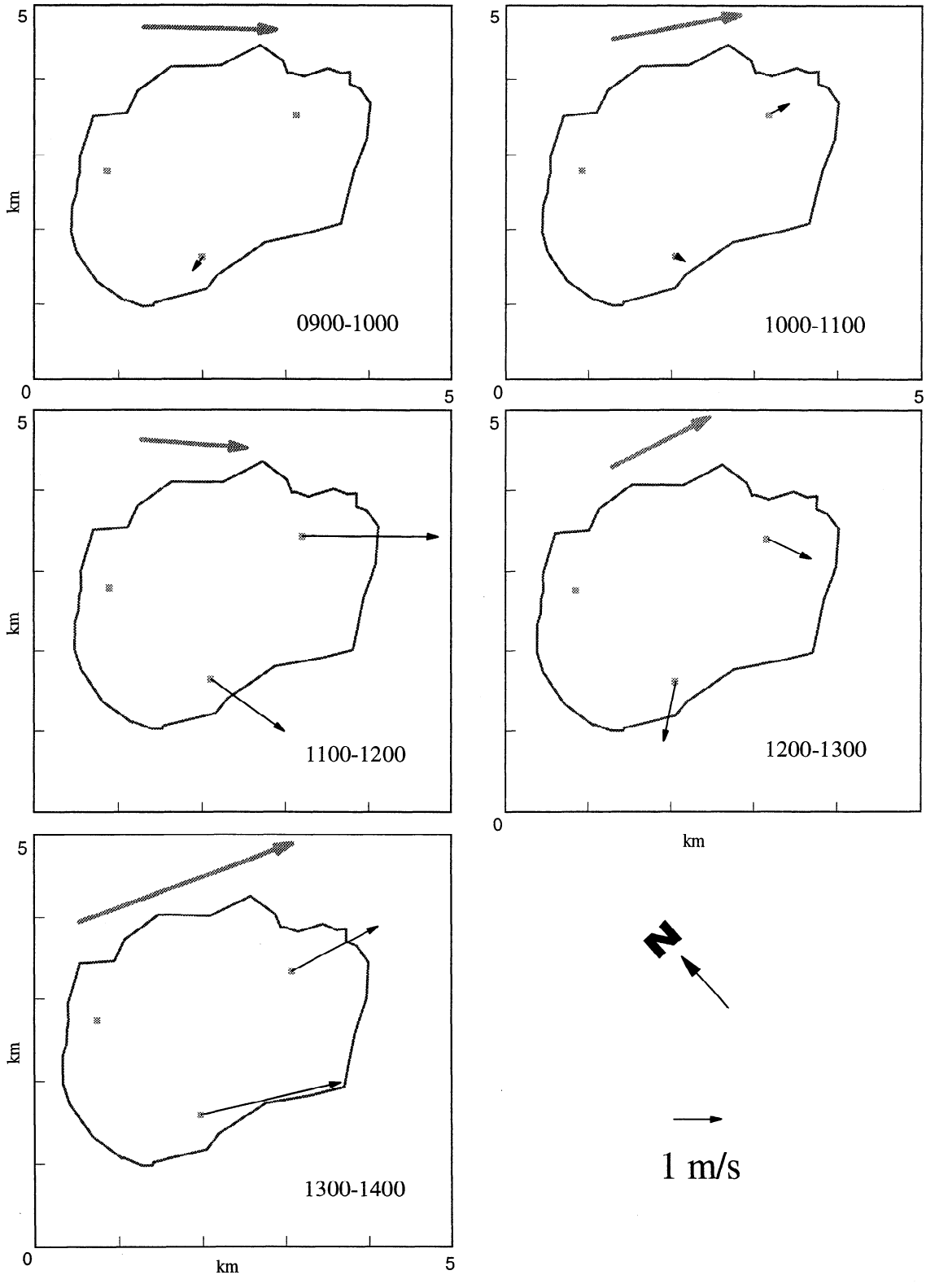

Figure 3. Hourly averaged wind vectors from the functioning anemometers on March 12. Also shown for each hour is the wind vector averaged from balloon observations between 45 m and 200 m.

The model PBL gains more sensible heat from the surface than observations would suggest (Figure 4). This is particularly so in the afternoon when conditions become cloudy, and the model significantly overestimates downwelling radiation. However, by 1300 a simple heat budget calculation suggests that when mixed up to the inversion at 1 km, this gives a warm bias in the model potential temperature of only 0.3 K. Later in the afternoon, the temperature bias in the simulated PBL becomes more pronounced (~ 1 K).

From Figure 6b, low-level onshore flow ~ 0.5 ms^{-1} is found in both the model and the observations at 1000. Also, the transition to offshore flow ~ 3 - 4 ms^{-1} above the stable layer at 50 m is well reproduced by the model. This encouraging comparison suggests that the modeled surface-induced

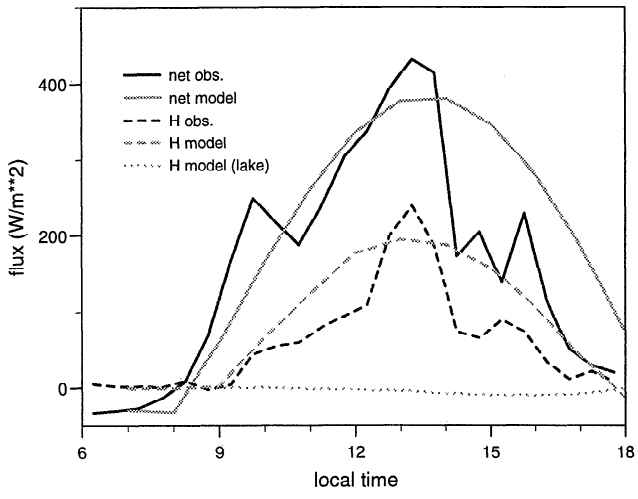

Figure 4. Observed and modeled net radiation and sensible heat flux (H) over the forest. The modeled sensible heat flux at the lake site is shown for reference.

pressure gradients over the lake are of a similar magnitude to those encountered on Namekus Lake on March 12. By 1300 the model indicates a well mixed momentum profile, with a magnitude similar to a local average of the rather noisy observed profile.

Comparison between modeled and observed contrasts in low-level temperature are shown in Figure 7. Prior to 1130, temperatures at the forest site are several degrees warmer than at the site 500 m downwind of the forest (northwestern (AWS) in Figure 7a) due to the variability in surface fluxes. This observed thermal gradient diminishes during early afternoon. However, a contrast ~ 3°C develops between the two lake sites around midday, despite being only 2 km apart. Both of these horizontal temperature contrasts are well represented by the model, although it should be remembered that the simulation develops a warm bias in the PBL.

4.4. Summary of Simulation

Initialized with a pronounced low-level inversion across the domain, the model illustrates how the flow develops

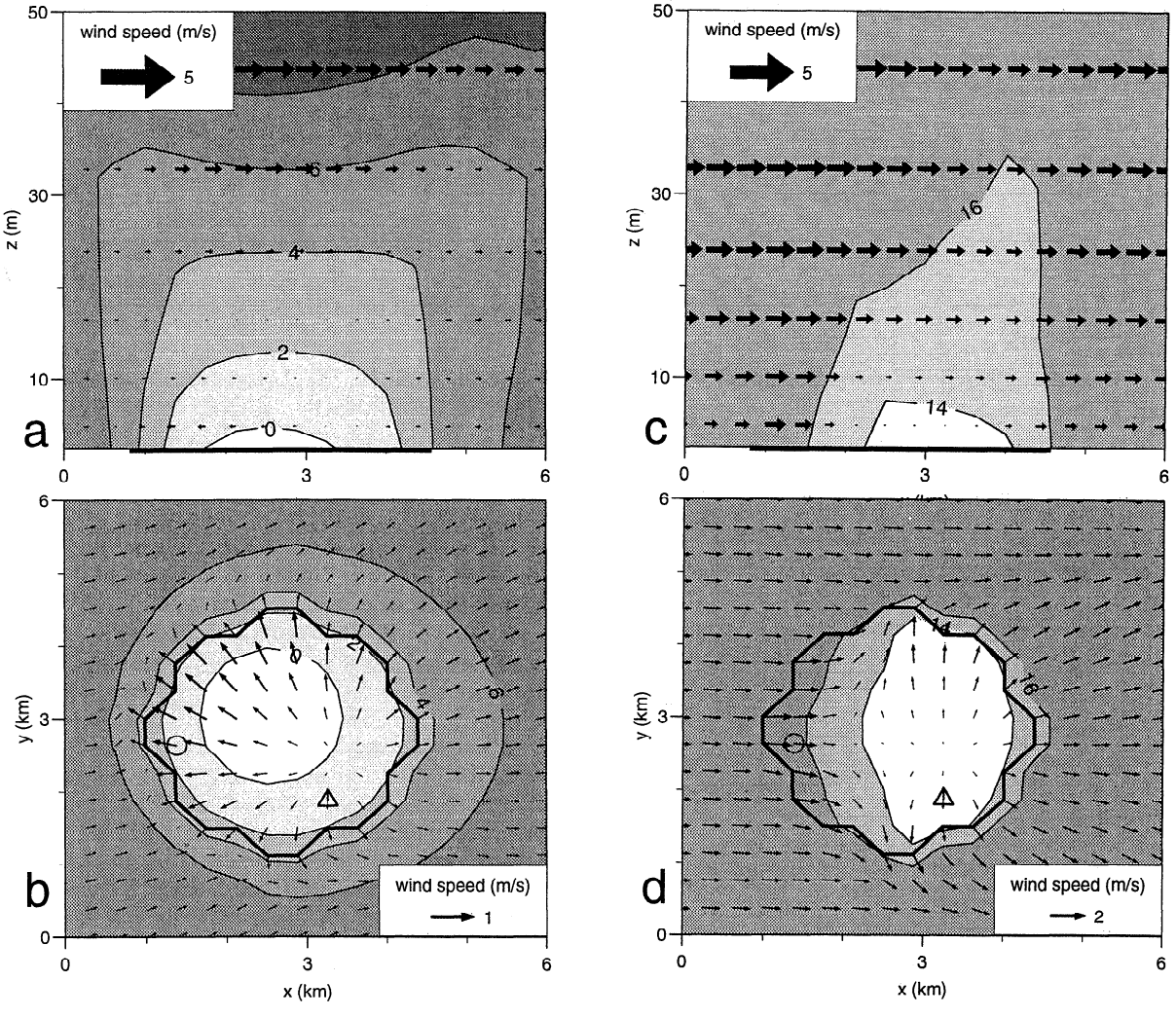

Figure 5. Model simulation showing potential temperature contours (°C) and three dimensional wind vectors at (a, b) 1000, (c, d) 1300, and (e, f) 1600. The vertical cross sections (a, c, e) are at y=3 km, and the plan views (b, d, f) are at 2.5 m, with the frozen lake indicated by the solid line. The circle and the triangle in the plan views indicate the location of the NW and SW AWS relative to the modeled wind direction.

across the lake under typical spring-melt conditions. Over the forest the inversion is destroyed by strong heating from the canopy. The warm and well mixed air is advected over very stable air extending several tens of meters above the lake. A snow breeze develops, with onshore flow exceeding 1 ms^{-1} around 1200 in the lowest 10 m. However, the advected forest air gradually erodes the lake inversion from above. By the afternoon, profiles are generally well mixed down to a few meters from the lake surface, depending on downwind distance from the forest. A poorly resolved but extremely stable layer remains just above the melting snow. Horizontal temperature gradients of several degrees persist across the lake throughout the afternoon, leading to a weak snow breeze effect at the downwind side of the lake. Modeled horizontal and vertical temperature gradients compare favorably with the observations. Reasonable agreement is also found between the available wind measurements and the model. These comparisons lend considerable weight to the ability of the model to capture the key atmospheric processes under these conditions.

5. Observations and Simulations Under Typical Conditions

5.1 Observations of Low-Level Flow

In the previous section we have chosen a single day to examine the development of a snow breeze given light winds and high insolation. We now seek to generalize these findings by analyzing the typical diurnal cycle of the low-level flow under a range of atmospheric conditions. While the balloon observations can provide useful measurements of the vertical structure above one point on the lake, ascents were only made on 7 days. Instead, we rely on the anemometer network which provided a complete data set of hourly wind speed and direction at a height of 2 m in three locations for 27 days (March 15 to April 11). This extends into the period when the snow and ice on the lake surface were rapidly melting and includes a range of typical atmospheric conditions. Low-level wind speed and radiation conditions are summarized by the bar charts in Figure 8. A daily averaged wind speed between 2 and 4 ms^{-1} was recorded on 16 of the 27 days. The daytime average incoming solar radiation exceeded 300 W m^{-2} with a similar frequency. For reference, the case study day of March 12 had somewhat weaker surface winds (1.6 ms^{-1}) and lower insolation (240 W m^{-2}) than the average for the period. A maximum daily average wind speed of 6.6 ms^{-1} was recorded on March 16, with blowing snow observed on the lake throughout the day. Shorter blowing snow episodes are likely to have occurred on a number of other days in the data set.

Figure 9 presents the mean wind speed at the northwestern site over the period as a function of time of day. There is a pronounced diurnal cycle, with speeds increasing by almost 3 ms^{-1} during the period 0900-1400. For the remainder of the afternoon, wind speeds remain relatively constant before

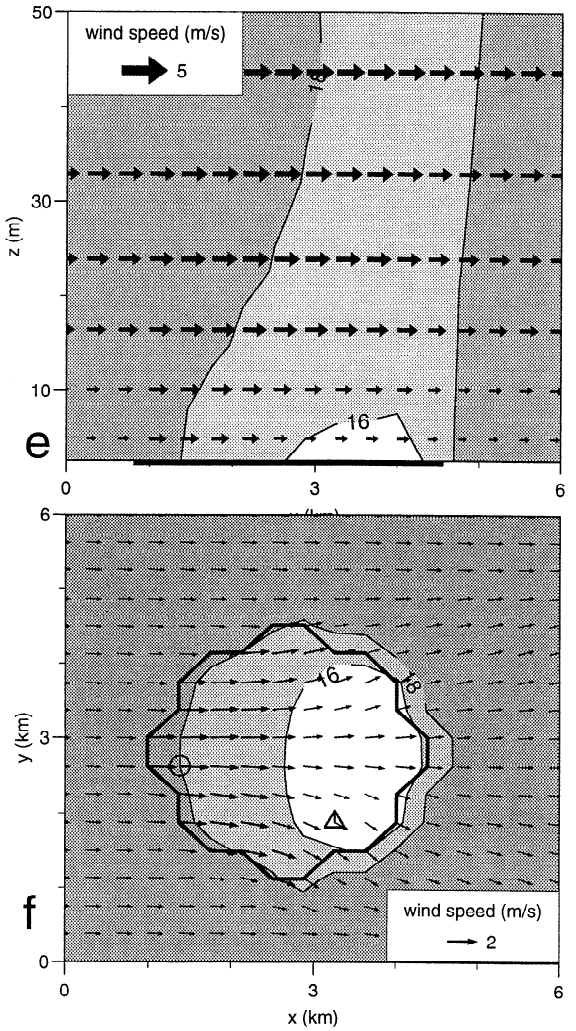

Figure 5. (continued)

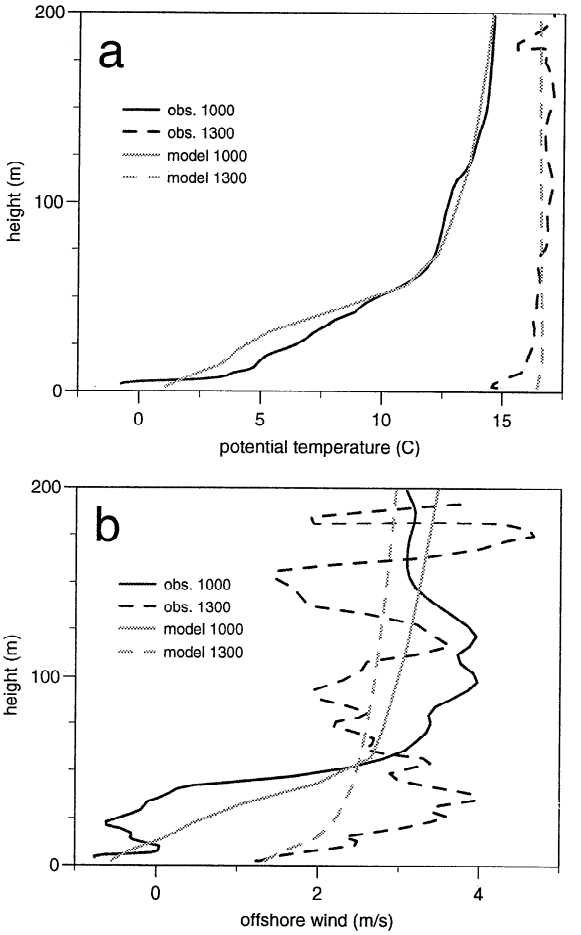

Figure 6. Observed and modeled profiles of (a) potential temperature and (b) offshore wind 750 m downwind of the forest-lake transition at 1000 and 1300.

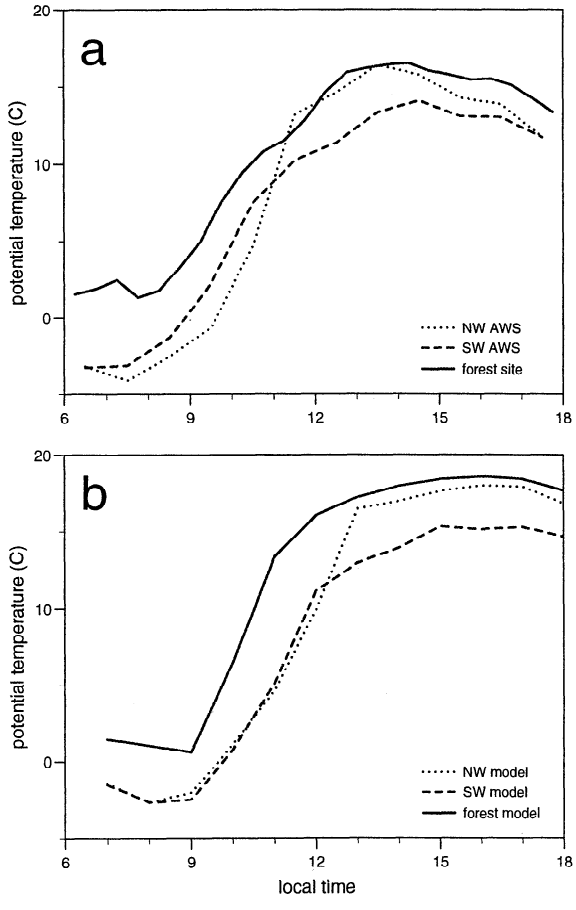

Figure 7. Evolution of temperature above surface as (a) observed by AWS at the forest and two lake sites and (b) modeled at an upwind forest point and at the corresponding locations on the lake.

dropping rapidly between 1900 and 2200. Winds then remain light throughout the night, until 1 - 2 hours after sunrise.

For the study of snow breezes the spatial variability in flow across the lake is more important than the mean wind speed. This variability can be characterized by the horizontal divergence of the wind, $\partial u/\partial x+\partial v/\partial y$. Given wind components u_1, u_2, and u_3 in the x direction located at (x_1,y_1), (x_2,y_2), and (x_3,y_3) respectively, and approximating u as a linearly varying function of x and y yields the following three equations:

$$\begin{aligned} u_1 &= u_0 + \alpha x_1 + \beta y_1 \\ u_2 &= u_0 + \alpha x_2 + \beta y_2 \\ u_3 &= u_0 + \alpha x_3 + \beta y_3 \end{aligned} \tag{10}$$

These equations can be solved to find α, equivalent to $\partial u/\partial x$. Adopting a similar procedure on the v component of the wind vector, the horizontal divergence can be expressed as

$$\frac{\partial u}{\partial x}+\frac{\partial v}{\partial y} = \frac{u_1(y_2-y_3)+u_2(y_3-y_1)+u_3(y_1-y_2)}{x_1(y_2-y_3)+x_2(y_3-y_1)+x_3(y_1-y_2)} + \frac{v_1(x_2-x_3)+v_2(x_3-x_1)+v_3(x_1-x_2)}{y_1(x_2-x_3)+y_2(x_3-x_1)+y_3(x_1-x_2)} \tag{11}$$

Using hourly values of u and v from each of the three sites, the divergence is calculated using the above expression and then averaged over all 27 days as a function of time of

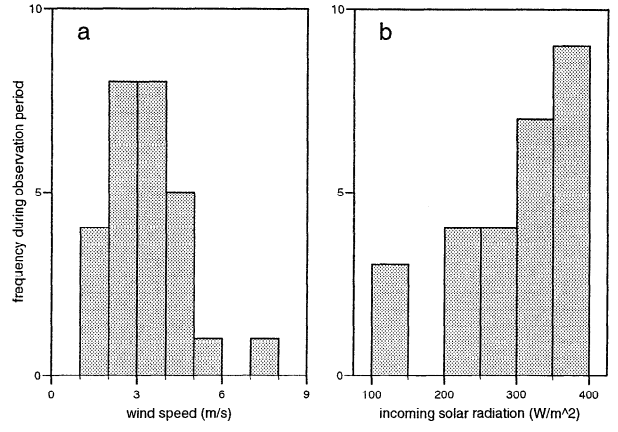

Figure 8. Histograms showing frequency of (a) wind speed and (b) incoming solar radiation conditions during the period March 15 - April 11, 1996. The wind speeds are meaned over all three sites and for every hour in the day, while the solar radiation is meaned over every hour between 0600 and 1900.

day (Figure 9). This produces a strong diurnal signal in phase with the wind speed. Divergence increases after 0800 and reaches a maximum an hour before solar noon (1300). As the maximum wind speed is reached in the afternoon, divergence over the lake drops steadily, with a rapid transition around 2000 to convergent nocturnal conditions.

The observations are now reanalyzed according to large-scale wind conditions. In the absence of wind speed observations well above the lake and forest canopy, the data are classified according to the daily average wind speeds from the three anemometers. Average diurnal cycles of the wind speed and divergence are presented in Figure 10 for the calmest and windiest five days of the observation period. These correspond to daily averaged 2 m wind speeds of less than 2.1 ms^{-1} and greater than 4.1 ms^{-1}, respectively. For the calmest days the amplitude and phase of the diurnal wind speed signal is very similar to the average wind speed while remaining about 2 ms^{-1} lighter. On the windiest days, diurnal trends in wind speed are less clear, though an increase in late morning is still evident. Examining the divergence patterns

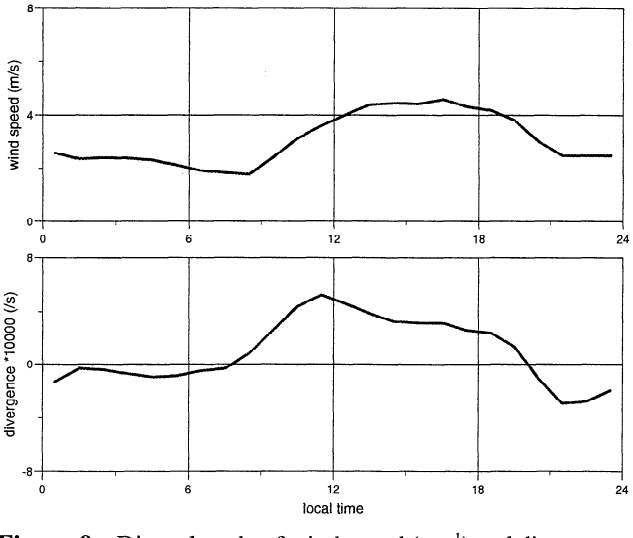

Figure 9. Diurnal cycle of wind speed (ms^{-1}) and divergence (x 10^4 s^{-1}) averaged over 27 days.

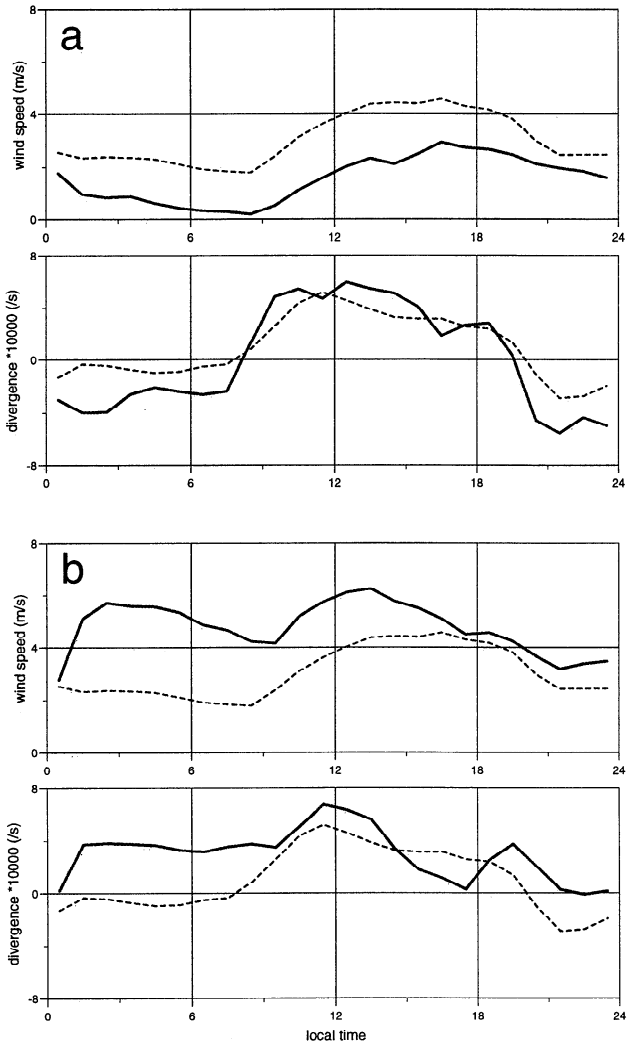

Figure 10. Observed wind speed (ms^{-1}) and divergence (s^{-1}) over the lake as a function of time of day averaged over (a) the five calmest and (b) the five windiest days. The average values over all 27 days are shown (thin lines) for reference.

for the calmest and windiest days, several features are apparent. On the calmer days the amplitude of the diurnal signal is more marked than on average. This is due to both strongly convergent flow at night and more divergent daytime conditions. On the windy days, there is a correlation between strongly divergent flow and wind speed.

The nature of the strongly divergent and convergent flows apparent in Figure 10 can be interpreted from analysis of the wind vectors across the lake. At each of the three sites, wind components are averaged over the data set for every hour of the day. These three sets of components are then linearly combined to produce a lake average wind vector, from which each of the three stations has a local deviation. The average and local deviation vectors across the lake are plotted in Figure 11a and 11b for the five calmest days in the data set. For clarity these have been averaged over two periods of 10 hours each, covering the strong daytime divergence and nighttime convergence apparent in Figure 10a.

The local perturbation vectors in Figure 11a are directed onshore during the day, a situation which is reversed at night (Figure 11b). This contrasts with the vectors in Figure 11c for the early morning divergent period on the five windiest days. Here the perturbation wind vectors are not clearly related to the direction of the nearest shoreline.

5.2. Simulations of Low-Level Flow Under Idealized Atmospheric Conditions

The numerical model is initialized here under idealized atmospheric conditions to help interpret the observations in the previous section. A constant potential temperature gradient $\partial\theta/\partial z$ and geostrophic wind profile are adopted for this study. Snow and vegetation temperatures are set at T_0, the temperature at the lowest atmospheric level of 2.5 m, and the forest canopy is assumed to be snow free. In the simulations described below, values of $\partial\theta/\partial z$=0.015 K m^{-1}, T_0=-21°C, and 50% relative humidity are used, with incoming solar radiation calculated by the short wave parameterization for March 21. The sensitivity of PBL flows to wind speed is illustrated with westerly geostrophic winds u_g of 2, 4, and 15 ms^{-1}. Note that even in the 15 ms^{-1} simulation, wind speeds at 10 m above the lake remain below the average dry snow threshold for blowing snow [*Li and Pomeroy*, 1997].

Figure 12 illustrates the horizontal wind and temperature fields over the lake at 2.5 m. As expected, the low-level flow is sensitive to the value of u_g. In the light wind case (u_g=2 ms^{-1}), horizontal temperature differences exceeding 2°C persist in the lowest 25 m. Consequently, the westerly flow

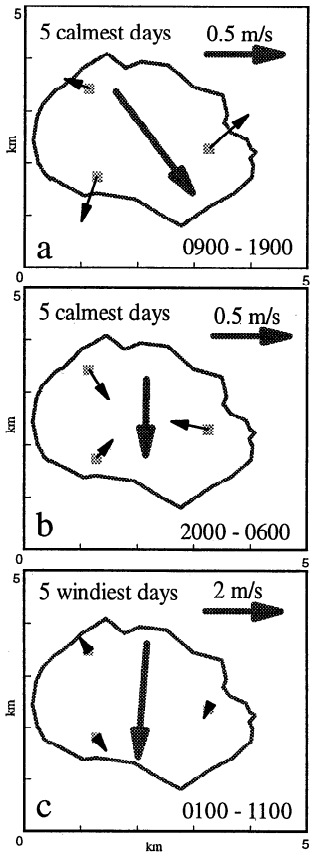

Figure 11. Wind vectors averaged over (a) daytime on the five calmest days, (b) night time on the five calmest days, and (c) the morning period on the five windiest days. The large vector at the center of the lake shows the mean conditions from the three sites, while the local perturbations are indicated at their respective locations on the lake.

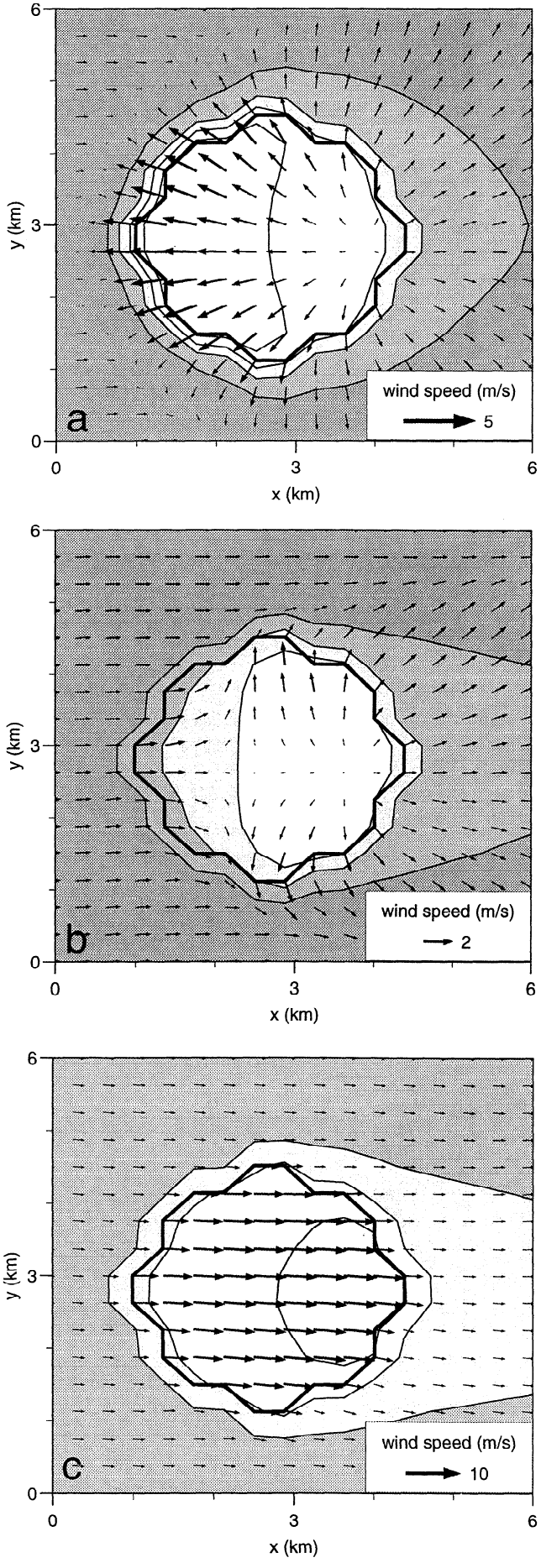

is strongly modified by a snow breeze which develops in the lowest 100 m above the lake. Onshore flow is found all across the lake, with the strongest components at the upwind edge. In the high wind case (Figure 12c, u_g=15 ms^{-1}), horizontal temperature contrasts of typically 1°C are found throughout the lowest 50 m, and the flow direction across the lake is uniform. Wind speeds increase downwind of the transition between the aerodynamically rough forest and the smooth frozen lake. In this case, the colder lake air is advected downwind into the forest, destroying the thermally induced pressure gradients which drive the snow breeze.

The flow for the intermediate wind speed simulation (Figure 12b, u_g=4 ms^{-1}) is qualitatively similar to the March 12 case study. A weak snow breeze develops in the lowest 25 m in the morning. By contrast with the u_g=2 ms^{-1} case, thermal gradients are weakened by turbulent mixing and advected eastward, resulting in only small perturbations to the flow downwind during the afternoon. The difference in snow breeze development between geostrophic winds of 2 and 4 ms^{-1} is in qualitative agreement with the simple scaling arguments proposed by *Segal and Arritt* [1992]. Given a midday surface heating contrast of 200 W m^{-2} around a patch of length scale 4 km, thermally induced flows counter geostrophic winds of less than approximately 2.5 ms^{-1}.

The evolution of the model flow over the lake is characterized in Figure 13, showing the average wind speed at 2.5 m averaged over every lake point for the duration of the simulation. The low-level wind speed for all three simulations shows marked diurnal variations. Under light winds (u_g=2 ms^{-1}) the pattern is associated with the snow breeze, giving a maximum speed at 1500, approximately 2 hours after solar noon. When u_g=15 ms^{-1}, the wind speed increases rapidly during the morning and remains close to 5 ms^{-1} throughout the afternoon. This behavior can be understood by examining the stability of the profile above the lake, as illustrated by the plot of average low-level Richardson number (*Ri*). Around 0900, warm forest air is advected over the lake, capping the cooler air beneath and preventing momentum transport down from aloft. Gradually, the lake inversion is eroded from above by vertical wind shear with *Ri* decreasing toward a neutral value of zero. Under these conditions momentum is transported down to the surface and wind speeds are large. In the evening, a stable layer redevelops and near-surface wind speeds consequently decrease. For the simulation where u_g=4 ms^{-1}, winds are dominated by the snow breeze in the morning and, increasingly, stability effects in the afternoon. The resulting areally averaged wind speed reflects this complex behavior.

Also shown in Figure 13 is the vertical convergence ($-\partial w/\partial z$) over the lowest atmospheric level, averaged over every lake grid point. By continuity, this quantity is approximately equal to the horizontal divergence over the lake ($\partial u/\partial x + \partial v/\partial y$) assuming that density gradients are small. For u_g=2 and 4 ms^{-1}, the shape of the curve is closely linked to the evolution of the snow breeze. This is illustrated in Figure 14 which shows vertical cross sections of vertical velocity over the lake at 1400. For u_g=2 ms^{-1}, the subsidence

Figure 12. Horizontal wind vectors and potential temperature contours (every 1°C) at a height of 2.5 m above the surface at 1400. The edge of the lake is denoted by the thick contour. (a) u_g=2ms^{-1}. (b) u_g=4 ms^{-1}. (c) u_g=15ms^{-1}.

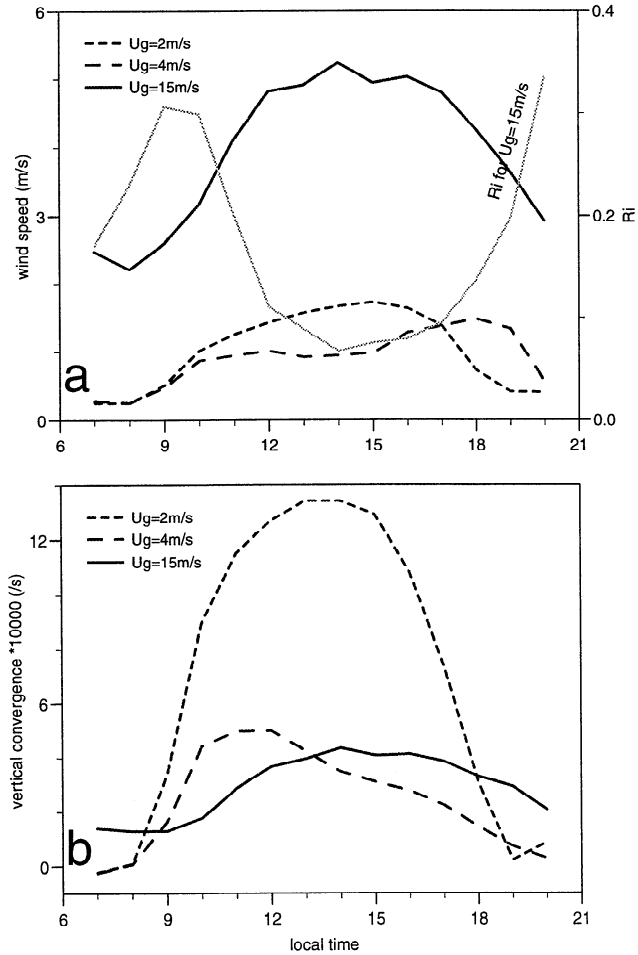

Figure 13. (a) Wind speed at 2.5 m and (b) vertical convergence over lowest 5 m, averaged over all lake grid points as a function of time of day for three values of geostrophic wind speed. The evolution of the lake-averaged Richardson number (*Ri*) between 2.5 and 7.6 m is shown for reference in Figure 13a for u_g=15 ms^{-1}.

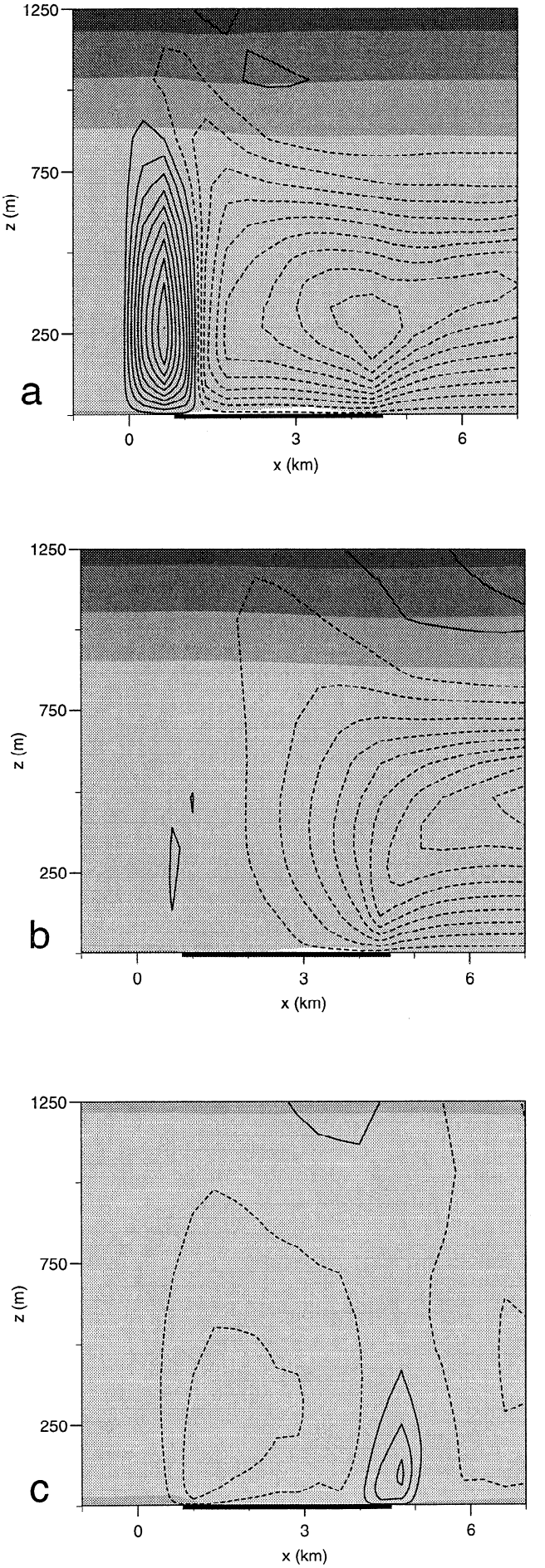

Figure 14. Vertical velocity contours every 4 cms^{-1} along the axis y=3 km at 1400 for (a) u_g=2 ms^{-1}, (b) u_g=4 ms^{-1}, and (c) u_g=15 ms^{-1}. Negative values are shown dashed. The location of the lake is marked by the thick line at z=0 m, and potential temperature contours every 2 K (shown by shading) indicate the depth of the mixed layer.

associated with the snow breeze is located over the lake. For u_g=4 ms^{-1} however, the circulation at the upwind edge of the lake has been destroyed. Weaker onshore flow remains on the downwind side of the lake at 1400 (evident from Figure 12b), and it is this that produces the downdraught located over the eastern half of the lake and beyond in Figure 14b. Because this weaker circulation has been advected downwind over the forest the vertical convergence averaged over the lake is further reduced relative to the u_g=2 ms^{-1} case. In both simulations the vertical velocity perturbations extend to the top of the PBL as can be seen from the (shaded) potential temperature contours, and their intensity is reflected in the near-surface values. The shorelines in the high wind simulation (Figure 14c) are associated with shallower vertical motion in the opposite directions to the snow breeze cases.

A downdraught at the upwind shore results from the acceleration of the low-level flow as it passes over the smoother lake. The wind subsequently decelerates as it reaches the rough forest, accompanied by ascent.

The observed divergence from the three anemometers (Figures 9 and 10) represents an areally averaged low-level vertical velocity over the lake and can be compared with the three simulations (Figure 13). In doing so, one must remember that the model flow is sensitive to the choice of imposed geostrophic wind. However, wind conditions above the surface layer in the observations are both unknown and time evolving.

From a qualitative viewpoint the diurnal cycle of the observations is a feature that is captured in the idealized simulations. Under light winds, horizontal divergence rises sharply. This is associated with onshore flow in both observations (Figure 11a) and the model (Figure 12a). Quantitatively, the observed divergence maximum under light winds is considerably smaller than in the idealized simulation with u_g=2 ms^{-1} and of similar magnitude to the case when u_g=4 ms^{-1}. Without knowledge of conditions in the upper PBL on observation days, interpretation of this comparison is difficult. Assuming that the model results are reasonable, it suggests that snow breezes do not typically persist over Namekus Lake through the entire day, as in the u_g=2 ms^{-1} case. The simulation with u_g=4 ms^{-1} may be more typical, with morning snow breezes weakening and being advected downwind in the afternoon. It should be noted however, that when wind speeds dropped and insolation was high, divergence of the magnitude simulated in the u_g=2 ms^{-1} case was recorded over several hours. However, such light synoptic winds did not persist for longer than a few hours during the observation period.

The observed nocturnal convergence over the lake on the five calmest days is not reproduced by the idealized simulations, and its origin is unclear. Measured fluxes over the lake and forest do not indicate any clear difference in heat fluxes after sunset, both remaining close to zero. The data show that offshore flow after sunset coincides with sudden decreases in wind speed. These events may be associated with a decoupling of the lake surface layer from the PBL. Under such calm conditions, it is possible that weak topographic flows can develop.

Under strong wind conditions, both the model and the observations suggest that divergence increases with wind speed. They also indicate that the local flow perturbations giving rise to divergence are largely in the direction of the wind aloft (Figures 11 and 12c). The low-level wind speed and divergence are less than in the observational data set. This may be due to the observations being made under windier PBL conditions than those represented by u_g=15 ms^{-1}. It may also be related to the effect of blowing snow episodes in the observations. The model is not valid under such conditions, when sensible heat fluxes into the lake may be considerably greater. A feature of the observations that is reproduced by the model is the increase in low-level wind speed (and divergence) during the morning. In the model this is related to the vertical transport of momentum down to the lake surface, controlled by stability effects associated with the nearby forest.

5.3. Sensitivity of Simulations to Initial Conditions

To place the interpretation of the observations from the idealized simulations in the context of typical flow conditions over Namekus Lake, sensitivities of the model to various atmospheric features should be highlighted. In particular, the low-level divergence over the lake is very sensitive to the choice of geostrophic wind speed. For decreasing values of geostrophic wind below u_g=5 ms^{-1}, divergence increases sharply, associated with a more intense snow breeze. At u_g=2 ms^{-1}, the downdraught remains coherent over the lake throughout the day. However, comparison with observations suggest that snow breezes over Namekus Lake tend to be weaker than this, particularly in the afternoon. For values of u_g above 5 ms^{-1} the maximum wind speed and divergence above the lake rise slowly with increasing geostrophic wind speed.

Other simulations with alternative temperature profiles have been made. The low-level flow was modified only slightly by halving the value of $\partial\theta/\partial z$, for example. The effect of raising daytime atmospheric temperatures above 0°C was also investigated by taking T_0=-1°C. Again, the trends in low-level wind speed and divergence remained unmodified, with only slight changes in their amplitudes. The snow breezes simulated are barely affected by this because the contrast in surface heating between the forest and the lake is fairly insensitive to the initial temperature. The thermal gradient is driven by the forest heat flux, which in this case is controlled by radiation rather than temperature. This demonstrates that the snow breeze is insensitive to whether the lake surface temperature is melting or is well below 0°C.

The snow breeze is sensitive to incoming radiation conditions which drive the forest heat flux. In the idealized experiments, the sky is cloud free, while observed short wave fluxes are often reduced by clouds. In addition, the presence of snow on the forest canopy reduces the observed sensible heat flux on a number of days. This results in a modeled heat flux that is 20% larger than the observations when averaged over all 27 days. However, the modeled and observed sensible heat fluxes compare very well under clear skies.

Additional simulations were made under midwinter radiation conditions (December 21). These indicate a weak snow breeze persists when u_g=2 ms^{-1}. It is unclear how frequent such midwinter snow breezes could occur over Namekus Lake. This is due to differences in the mid-winter forest energy budget compared with the model and, in particular, the role of interception and albedo at low Sun angles. For calm days in March however, the existence of snow breezes in low-insolation conditions was confirmed by observational evidence from both the tethered balloon profiles and the anemometer network. These indicated snow breeze development when the mixed layer wind speed dropped to 1 ms^{-1} for several hours. This occurred on a day when incoming solar radiation remained around 200 Wm^{-2}, approximately 30% of typical clear-sky values for March.

The value of 1 mm for the lake roughness length was adopted as a reasonable estimate from a long time series of observations. However, the roughness of the snow-covered lake does vary over time, due to ageing of the snow, development of drifts, etc. Simulations using an alternative value of roughness length of 10 mm produced very similar divergent flows. One should note that areas of open wetlands and encroaching farmland can also be characterized by roughness lengths of this magnitude when snow is on the ground. In this case, the energy balance is similar to that of a snow-covered lake. Snow breezes of a similar magnitude

are therefore likely to develop over patches of clear-cut as well as around lakes.

6. Conclusions

This study has shown how snow breezes affect the low-level wind field over a frozen, snow-covered lake less than 4 km across within the boreal forest. Examining the average diurnal conditions over a period of 27 days in March and April, a snow breeze signal is evident during the morning period. This thermally induced influence on the low-level wind weakens in the afternoon. With clear skies, snow-free canopies, and under calmer conditions (wind speeds ~ 2 ms^{-1}), the snow breeze will persist throughout the day. However, snow breeze effects are not in evidence on the windiest days. In this case, the low-level wind accelerates across the lake due to the contrast in roughness between the forest and the lake. There is no clear effect of ambient temperature on the development of snow breezes across Namekus Lake, despite the extremely stable conditions associated with temperatures above 0°C over the lake.

The intensity of NCMCs is expected to be very sensitive to the length scale of heterogeneity. For example, observations by *Segal and Kubesh* [1996] indicate that thermally induced winds as strong as 6 ms^{-1} develop around the much larger frozen lake Winnipeg. This study has shown that circulations, albeit weak ones, still develop over a snow-covered lake only a few kilometers across. This is due to the extreme contrast in surface features over the boreal forest during winter. The heterogeneity may be naturally occurring, due to frozen lakes and wetlands, or man-made as in the case of forest cleared for agriculture. Between them, these surfaces account for typically 25% of the landscape in this part of Canada and occur at a range of length scales. This suggests that snow breezes are widespread throughout the region during the winter.

Acknowledgments. This work was supported financially by the NERC through its TIGER (Terrestrial Initiatives in Global Environmental Research) Program, award GST/91/III.2/2A, through BOREAS contract NAG-52302, the Prince Albert Model Forest Association Inc., Atmospheric Environment Service, Climate Research Network, Mackenzie Basin Global Energy and Water Cycling Experiment, National Hydrology Research Institute, Environment Canada, and the Division of Hydrology, University of Saskatchewan, Saskatoon. The authors would also like to thank Newell Hedstrom, Dell Bayne, and Mike Stroud for their assistance in the field.

References

Chang, J. T., and P. J. Wetzel, Effects of spatial variations of soil moisture and vegetation on the evolution of a prestorm environment—A numerical case-study, *Mon. Weather Rev.*, **119**, 1368-1390, 1991.

Chen, F., and R. Avissar, Impact of land-surface moisture variability on local shallow convective cumulus and precipitation in large-scale models, *J. Appl. Meteorol.*, **33**, 1382-1401, 1994.

Dalu, G. A., R. A. Pielke, R. Avissar, G. Kallos, M. Baldi, and A. Guerrini, Linear impact of thermal inhomogeneities on mesoscale atmospheric flow with zero synoptic wind, *Ann. Geophys.*, **9**, 641-647, 1991.

Harding, R. J., and J. W. Pomeroy, Energy-balance of the winter boreal landscape, *J. Clim.*, **9**, 2778-2787, 1996.

Li, L. and J.W. Pomeroy, Estimates of threshold wind speeds for snow transport using meteorological data, *J. Appl. Meteorol.*, **36**, 205-213, 1997.

Louis, J. F., M. Tiedke, and J. F. Geleyn, A short history of the PBL parameterization at the ECMWF, in *Workshop on Planetary Boundary Layer Parameterization*, 59-80, Eur. Cent. for Medium-Range Weather Forecasts, Reading, England, 1981.

Lynn, B. H., D. Rind, and R. Avissar, The importance of mesoscale circulations generated by subgrid-scale landscape heterogeneities in general-circulation models, *J. Clim.*, **8**, 191-205, 1995.

Mahfouf, J. F., E. Richard, and P. Mascart, The influence of soil and vegetation on the development of mesoscale circulations, *J. Clim. Appl. Meteorol.*, **26**, 1483-1495, 1987.

Mahrt, L., J. L. Sun, D. Vickers, J. I. MacPherson, J. R. Pederson, and R. L. Desjardins, Observations of fluxes and inland breezes over a heterogeneous surface, *J. Atmos. Sci.*, **51**, 2484-2499, 1994.

Male, D. H. and R. J. Granger, Snow surface energy exchange, *Water Resour. Res.*, **17**, 609-627, 1981.

Mason, P. J., The formation of areally-averaged roughness lengths, *Q. J. R. Meteorol. Soc.*, 399-420, 1988.

McNider, R. T., and R. A. Pielke, Diurnal boundary-layer development over sloping terrain, *J. Atmos. Sci.*, **38**, 2198-2212, 1981.

Ookouchi, Y., M. Segal, R. C. Kessler, and R. A. Pielke, Evaluation of soil moisture effects on the generation and modification of mesoscale circulations, *Mon. Weather Rev.*, **112**, 2281-2292, 1984.

Pielke, R. A., G. A. Dalu, J. S. Snook, T. J. Lee, and T. G. F. Kittel, Nonlinear influence of mesoscale land-use on weather and climate, *J. Clim.*, **4**, 1053-1069, 1991.

Pielke, R. A., *et al.*, A comprehensive meteorological modeling system—RAMS, *Meteorol. Atmos. Phys.* **49**, 69-91, 1992.

Pinty, J. P., P. Mascart, E. Richard, and R. Rosset, An investigation of mesoscale flows induced by vegetation inhomogeneities using an evapotranspiration model calibrated against HAPEX-MOBILHY data, *J. Appl. Meteorol.*, **28**, 976-992, 1989.

Pomeroy, J.W. and K. Dion, Winter radiation extinction and reflection in a boreal pine canopy: Measurements and modelling, *Hydrol. Processes*, 10, 1591-1608, 1996.

Raupach, M. R., and J. J. Finnigan, Scale issues in boundary-layer meteorology: surface energy balances in heterogeneous terrain, *Hydrol. Process.*, **9**, 589-612, 1995.

Segal, M., and R. W. Arritt, Nonclassical mesoscale circulations caused by surface sensible heat-flux gradients, *Bull. Am. Meteorol. Soc.*, **73**, 1593-1604, 1992.

Segal, M., and R. Kubesh, Inferring snow-breeze characteristics from frozen-lake breezes, *J. Appl. Meteorol.*, **35**, 1033-1039, 1996.

Segal, M., R. Avissar, M. C. Mccumber, and R. A. Pielke, Evaluation of vegetation effects on the generation and modification of mesoscale circulations, *J. Atmos. Sci.*, **45**, 2268-2292, 1988.

Segal, M., W. E. Schreiber, G. Kallos, J. R. Garratt, A. Rodi, J. Weaver, and R. A. Pielke, The impact of crop areas in Northeast Colorado on midsummer mesoscale thermal circulations, *Mon. Weather Rev.*, **117**, 809-825, 1989.

Segal, M., J. H. Cramer, R. A. Pielke, J. R. Garratt, and P. Hildebrand, Observational evaluation of the snow breeze, *Mon. Weather Rev.*, **119**, 412-424, 1991a.

Segal, M., J. R. Garratt, R. A. Pielke, and Z. Ye, Scaling and numerical-model evaluation of snow-cover effects on the generation and modification of daytime mesoscale circulations, *J. Atmos. Sci.*, **48**, 1024-1042, 1991b.

Sellers, P., *et al.*, The boreal ecosystem-atmosphere study (BOREAS)—An overview and early results from the 1994 field year, *Bull. Am. Meteorol. Soc.*, **76**, 1549-1577, 1995.

Shuttleworth, W. J., Macrohydrology—The new challenge for process hydrology, *J. Hydrol.*, **100**, 31-56, 1988.

Smagorinsky, J., General circulation experiments with the primitive equations, 1, The basic experiment, *Mon. Weather Rev.*, **91**, 99-164, 1963.

Smith, E. A., M. M. K. Wai, H. J. Cooper, and M. T. Rubes, Linking boundary-layer circulations and surface processes during FIFE-89, 1, Observational analysis, *J. Atmos. Sci.*, **51**, 1497-1529, 1994.

Sun, J.L., D.H. Lenschow, L. Mahrt, T.L. Crawford, K.J. Davis,

S.P. Oncley, J.I. MacPherson, Q. Wang, R.J. Dobosy, and R.L. Desjardins, Lake-induced atmospheric circulations during BOREAS, *J. Geophy. Res.*, **102**, 29,155-29,166, 1997.

Sun, W. Y., and Y. Ogura, Boundary-layer forcing as a possible trigger to a squall-line formation, *J. Atmos. Sci.*, **36**, 235-254, 1979.

Vidale, P.L., R.A. Pielke, L.T. Steyaert, and A. Barr, Case study modeling of turbulent and mesoscale fluxes over the BOREAS region, *J. Geophy. Res.*, **102**, 29,167-29,188, 1997.

Walko, R.L., *et al.*, Coupled atmosphere-terrestrial ecosystem-hydrology models for environmental modeling. Class Report #9, Dept. of Atmos. Sci., Colorado State Univ., Fort Collins, CO 1998.

Zeng, X. B., and R. A. Pielke, Landscape-induced atmospheric flow and its parameterization in large-scale numerical-models, *J. Clim.*, **8**, 1156-1177, 1995.

Zhong, S., and J. C. Doran, A study of the effects of spatially varying fluxes on cloud formation and boundary layer properties using data from the Southern Great Plains Cloud and Radiation Testbed, *J. Clim.*, **10**, 327-341, 1997.

C. M. Taylor and R. J. Harding, Institute of Hydrology, Crowmarsh Gifford, Wallingford, Oxfordshire, U.K. (e-mail; cmt@ioh.ac.uk; rjh@ioh.ac.uk)

R. A. Pielke, P. L. Vidale and R. L. Walko, Department of Atmospheric Science, Colorado State University, Fort Collins, CO 80521. (e-mail: tara@romulan.atmos.colostate.edu; vidale@homebrew.atmos.colostate.edu; walko@tibet.atmos.colostate,edu)

J. W. Pomeroy, National Hydrology Research Institute, Saskatoon, Canada (e-mail: pomeroyj@nhrisu.nhrc.sk.ec.gc.ca

(Received October 21, 1997; revised April 6, 1998;
accepted May 8, 1998.)